Characteristics of adaptive network-based fuzzy inference system for typhoon inundation level forecast

Huei-Tau Ouyang

ABSTRACT

Heavy rainfall brought in by a typhoon often causes severe inundation in a low-lying area. Due to budget constraints, inundation level monitoring programs often cease to continue after the project ends. In such cases, forecast models capable of predicting inundation levels solely based on rainfall data to provide supportive information for responding actions during typhoons are urged. This paper aims to explore two types of typhoon inundation level forecast models based on adaptive network-based fuzzy inference system (ANFIS): one employing only rainfall data as inputs (ANFIS-R) to cope with the situation where water level observation is lacking, and the other one using both rainfall and water level data as inputs (ANFIS-B). A methodology is proposed to identify the appropriate time interval of rainfall accumulation to be used as model inputs. The forecast capacities of the models are assessed in three aspects: prediction accuracy, peak level error, and time shift error. The proposed ANFIS models are compared with traditional ARX-based models. The results show that ANFIS-B models outperform ARX-based models on all three aspects. ANFIS-R models display comparable prediction accuracy and superior performance on peak level forecast and time shift error. This renders ANFIS-R models promising in areas lacking water level observations.

Key words | ANFIS, forecast, inundation, typhoon, water-level

Huei-Tau Ouyang
Department of Civil Engineering,
National Ilan University,
Yilan 26047,
Taiwan
E-mail: *htouyang@niu.edu.tw*

INTRODUCTION

Typhoon is a type of tropical cyclone that develops in the western part of the North Pacific Ocean between 180 and 100 °E and usually emerges in the area near Taiwan during the period from June to October. During the events, heavy rainfall carried in by typhoons often leads to severe inundation in low-lying areas. To effectively issue early warnings and damage mitigation operations for typhoon invasion, accurate forecasting on the inundation depth in the area with a few hours of lead time is crucial. However, due to limitations in project funding, inundation level monitoring programs often cease to carry on after the project has ended. To provide supportive information for responding actions during typhoons, demands have arisen for forecast models that are capable of predicting inundation levels based only on rainfall data. To this end, the purpose of the present study is to explore the possibility of developing inundation level forecasting models solely based on rainfall data and to compare the prediction capacity of such models with those in both rainfall and water level data as inputs.

The common inundation forecasting techniques can generally be divided into two approaches: numerical simulation and black-box modeling. In numerical simulations, the mechanisms that cause inundation are obtained through theoretical derivations based on physical laws. Supported by theoretical grounds, numerical simulations can usually provide a solid foundation to explain the causal relationship between rainfall and inundation level. However, a numerical model usually requires a considerable amount of computing time and machine resources for the simulations,

doi: 10.2166/nh.2017.009

making it hard to provide forecast information in real-time to support immediate response during a typhoon. Also, substantially more data are required to specify the physical characteristics of the system for numerical models. Black-box modeling takes a completely different approach. In black-box modeling, the relationship between rainfall and inundation level is viewed as a black-box system. Without probing into the complicated underlying physical mechanisms, black-box modeling focuses on accurately simulating the relationship between inputs and outputs of the system. Although this approach is not capable of explaining the physical mechanisms of inundation, it can quickly provide forecasts with high accuracy that are usually comparable to the results obtained by physical-based models. This real-time forecasting capability supports the potential practice of these models in disaster prevention operations during typhoons.

So far, a large number of studies in the literature have applied black-box modeling to develop forecasting models. For instance, Chang & Chang (2006) developed a neuro-fuzzy hybrid approach to constructing a water level forecasting system during flood periods. Mousavi *et al.* (2007) compared the methods of ordinary least-squares regression, fuzzy regression (FR), and adaptive network-based fuzzy inference system (ANFIS) in inferring operating rules for a reservoir operation optimization problem, and concluded that FR is useful to derive operating rules for a long-term planning model and ANFIS is beneficial in medium-term implicit stochastic optimization. Napolitano *et al.* (2010) utilized an adaptive conceptual model and an artificial neural network (ANN) to develop a real-time forecasting system capable of predicting hourly water levels at Ripetta stream gauging station in Rome. Moeini *et al.* (2011) presented a fuzzy rule-based model for the operation of hydropower reservoirs and demonstrated the superiority of the developed model over a traditional stochastic dynamic programming approach. Li *et al.* (2015) applied back-propagation neural network (BPNN) to simulate water-level variations of a large lake, and achieved results with comparable accuracies to a 2D hydrodynamic model. Fayaed *et al.* (2015) developed a comprehensive modified stochastic dynamic programming with an artificial neural network (MSDP-ANN) model to derive optimal operational strategies for a reservoir and demonstrated that the MSDP-ANN produces a more reliable and resilient model and a smaller supply deficit. Granata *et al.* (2016) compared rainfall-runoff modelings between a support vector regression (SVR) approach and the EPA's Storm Water Management Model (SWMM). Their results showed that the SVR algorithm tends to underestimate the peak discharge. Babel *et al.* (2016) employed an ANN technique to forecast seasonal rainfall and to determine the effects of climate change on rainfall. They also demonstrated that the developed models are able to forecast rainfall one to two months in advance. Feng *et al.* (2016) developed an extreme learning machine and generalized regression neural network models for maize ET estimation. Li *et al.* (2016) compared the prediction capacity of a multiple linear regression (MLR), BPNN and support vector machine (SVM), and concluded that the SVM model optimized by particle swarm optimization was superior to MLR and BPNN. Gorgij *et al.* (2016) developed a hybrid wavelet-ANN-GP model for groundwater budget forecasting and demonstrated the prediction capacity of the model via a case study in Iran. Yin *et al.* (2016) investigated the accuracy of integrating a genetic algorithm and SVM models for simulating daily reference evapotranspiration. Their results showed that the developed methodology outperforms SVM and feed-forward ANN models. Zounemat-Kermani (2016) compared forecasting models for suspended sediment concentration in streamflow based on artificial neural networks with Levenberg–Marquardt (ANN-LM), particle swarm optimization learning algorithms (ANN-PSO), ANFIS, and gene expression programming. The results show that data-driven models are significantly superior to trajectory-based models. Group method of data handling has been recently applied in various environmental and hydrologic sciences, such as predicting longitudinal dispersion in water networks (Najafzadeh & Sattar 2015; Najafzadeh & Bonakdari 2016; Najafzadeh & Tafarojnoruz 2016).

From the above review of related works, it appears that studies applying an ANFIS to the forecasting of inundation level for typhoons are relatively rare. It is new and topical for further study. The purpose of this paper aims to explore the characteristics of ANFIS-based models for typhoon inundation level forecast. Two types of ANFIS models are proposed. The first one uses only rainfall data as inputs (named ANFIS-R hereafter), corresponding to the cases

where the inundation level monitoring programs have ceased to continue. The second type (named ANFIS-B), as a comparison to ANFIS-R, utilizes both rainfall and water level data as inputs. The performance of both types of models is evaluated by assessing the accuracy of the predicted hydrograph, the error in peak water level, and the time lag of the predicted water level. The remainder of this paper is organized as follows: the following section introduces the environmental background of the study area. The ANFIS models are then described, the choice of input variables, and the assessing indices of model performance. The next section discusses the characteristics of the proposed ANFIS-based models, the comparison of model performances to other approaches, and the model sensitivities to the uncertainties rooted in the inputs of rainfall and water level. Finally, the conclusions are drawn based on the findings.

STUDY REGION AND DATA

Yilan County (as shown in Figure 1), located in northeastern Taiwan, has a subtropical monsoon climate and is known for its rainy weather. With over 200 rainy days a year, the area has an annual average precipitation of 2,000–2,500 mm. During the seasons of summer and fall, the area is exposed to high risk of typhoon invasions. Statistics show that Taiwan is hit by an average of 2–3 typhoons each year, and 45% of these typhoons make landfall in Yilan County (Pan *et al.* 2014; Ouyang 2016a, 2016b). Due to the rainy environment and the proneness to typhoons, low-lying areas in Yilan County often suffer serious inundation, among which the Donsan area (as shown in Figure 1) is one of the regions that are most prone to inundation. The area is flat and the averaged ground elevation is only about 2 m above sea level. During the period of a typhoon invasion, the rapid accumulation of surface runoff usually results in disastrous flooding and serious damage in the area within a short time.

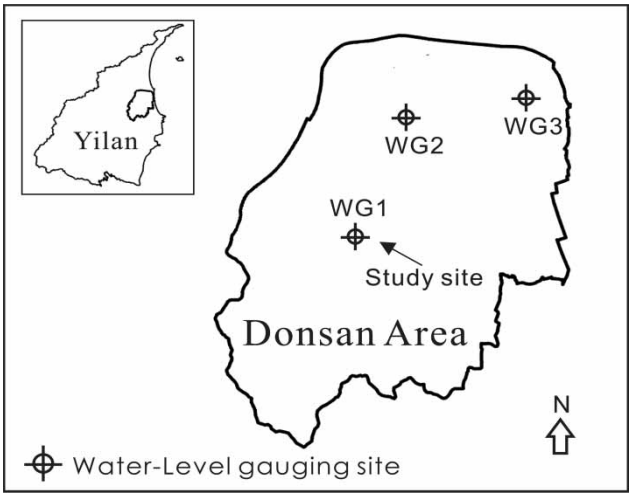

Figure 1 | Donsan area in Yilan County, Taiwan.

In order to acquire a better understanding of inundation in Donsan area during typhoons, a typhoon inundation surveillance system was set up by Taiwan Water Resources Agency in 2012. The system consists of three water-level gauging stations and a data transmission interface that can retrieve precipitation observations from QPESUMS (Quantitative Precipitation Estimation and Segregation Using Multiple Sensor, Gourley *et al.* 2002) of Taiwan Central Weather Bureau (TCWB). The gauging stations are located as shown in Figure 1. In the event of a typhoon, the gauging network reports the inundation level at the site every 10 minutes by means of radio transmission, and the data transmission interface receives the 10-minute rainfall data from QPESUMS via the Internet at the same frequency. QPESUMS was jointly established by TCWB and the National Severe Storm Laboratory (NSSL) in 2002 with an objective to improve the forecast accuracy of quantitative rainfall. QPESUMS also provides precipitation forecasts up to 72 hours ahead by predicting the movement paths of cloud cells.

Since its implementation, this surveillance system has collected data from eight typhoon events, as listed in Table 1. Figure 2 demonstrates the water levels recorded at the three gauging stations and the rainfall data from QPESUMS during Typhoon Usagi in 2013. These data not only provide the real-time inundation information on-site of the area during each typhoon but also can be utilized to develop water level forecasting models. Preliminary studies indicated that, among all the gauging stations in the surveillance system, data from WG1 has shown the best results. Thus, WG1 is selected as the study target in the present study.

Table 1 | Historical typhoon events recorded in Donsan area

Typhoon	Year	Time of official typhoon sea warning issued h/day/month (UTC)	Affecting period (h)	Cumulative rainfall (mm)	Maximum rainfall intensity (mm/h)
Saola	2012	2030/30/Jul	90	537.4	37.4
Soulik	2013	0830/11/Jul	63	133.3	29.9
Trami	2013	1130/20/Aug	45	161.3	22.2
Usagi	2013	2330/20/Sep	63	168.7	23.2
Matmo	2014	1730/21/Jul	54	97.5	35.7
Fung-wong	2014	0830/19/Sep	72	72.4	40.9
Soudelor	2015	1130/6/Aug	69	421.1	87.6
Dujuan	2015	0830/27/Sep	57	217.9	42.1

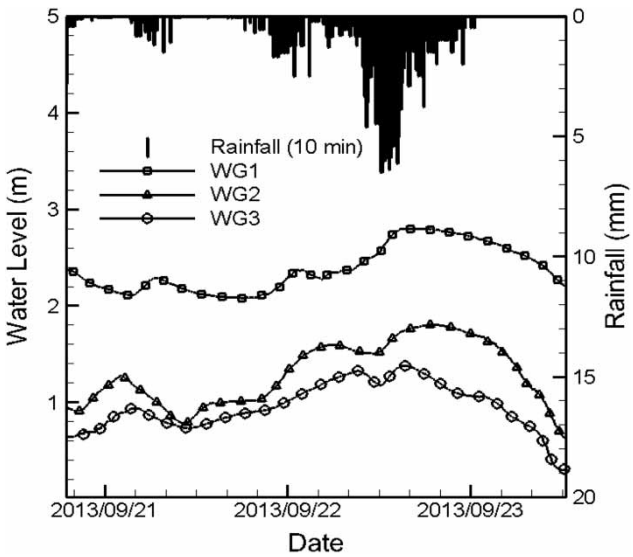

Figure 2 | Rainfall and water-level data recorded in Donsan area during typhoon Usagi.

METHODS

ANFIS models

The early development of a fuzzy inference system (FIS) can be dated back to the fuzzy logic research of Marinos (1969). After Zadeh (1971) introduced the concept of fuzzy inference, fuzzy theory became a popular research topic. Mamdani's (1974) use of logical conditions further consolidated the theoretical foundation of fuzzy theory. Jang (1993) proposed a network architecture of FIS that integrates a learning algorithm for self-calibration of model parameters and named it Adaptive Network-based Fuzzy Inference System (ANFIS). Through this feature of self-learning, ANFIS is able to capture the essence of the input–output relationship of a system with high accuracy.

ANFIS consists of two components, one is Takagi & Sugeno's (1985) Fuzzy Inference System (TS-FIS) and the other is an algorithm that assimilates the learning capability of ANN. In TS-FIS, the rule consequents usually consist of crisp numbers or linear functions of inputs, as shown in the following equation:

$$\text{IF } x \text{ is } A_i \text{ THEN } y_i = a_i^T x + b_i \quad i = 1, 2, \ldots, M \tag{1}$$

where the IF part is called the antecedent, and the THEN part is named the consequent; x is an input in the antecedent part, and y_i is the output in the consequent part; a_i and b_i are parameters in the consequent part; M denotes the number of rules, and A_i indicates the antecedent fuzzy membership function value of the ith rule. The membership function can be triangular, trapezoidal, Gaussian, bell, sigmoidal, etc., depending on the goodness of fit for model simulation. For example, the Gaussian membership function has the following form:

$$f(x) = e^{-(x-c)^2/2\sigma^2} \tag{2}$$

where σ and c are parameters to be calibrated.

For the second component of ANFIS, Jang (1993) proposed a network architecture of TS-FIS integrated with the error propagation algorithm assimilated from ANN. By comparing the simulation results of TS-FIS and the data, ANFIS can automatically calibrate the parameters in the antecedent and the consequent parts to progressively adjust outputs closer to the data. In ANFIS, the parameters in the antecedent part are adjusted using the back-propagation algorithm similar to ANN, and the parameters in the consequent part are adjusted using the least square algorithm. Details on the ANFIS can be found in the related literature (Jang 1993; Chang & Chang 2001, 2006; Chang *et al.* 2005).

Analysis of rainfall data

To determine the proper inputs for the model, the relationship between rainfall and water level at the study site was first

analyzed by conducting a cross-correlation analysis. The correlation coefficient (CC) is defined as follows (Gayen 1951):

$$\mathrm{CC(x,\,y)} = \frac{cov(x,\,y)}{\sigma_x \sigma_y} = \frac{\sum_{i=1}^{n}(x_i - \bar{x})(y_i - \bar{y})}{\sqrt{\sum_{i=1}^{n}(x_i - \bar{x})^2}\sqrt{\sum_{i=1}^{n}(y_i - \bar{y})^2}} \quad (3)$$

where *cov* denotes the covariance between x and y, σ_x and σ_y are respectively the standard deviations of x and y, and n is the number of observations. CC ranges between -1 and 1. CC $= 1$ indicates a completely positive correlation between x and y while CC $= -1$ denotes completely negative correlation, and CC $= 0$ indicates no correlation between x and y.

As both the precipitation and water level data are recorded in a 10-minute frequency, the cross-correlations between the water level data and the 10-minute rainfall increments over various lags were first calculated for all the typhoon events. The results are as shown in Figure 3, the circle dots indicate the mean CC averaged over all events, and the error bars above and below indicate respectively the maximum and minimum CCs in all events. As shown in the figure, it appears that the correlations between water level and 10-minute increment of rainfall are not very prominent. For all the time lags tested, the average CCs are all below 0.5 and the maximums never pass above 0.6. This suggests that the 10-minute increment of rainfall might not be a proper variable to be used as a model input.

Since the terrain in the study area is very flat, the variation in inundation level is usually not as swift as rainfall, and a certain amount of time is often required for the water to build up. This suggests that the water level in the area might be correlated more to rainfall accumulation, rather than 10-minute rainfall increments. To determine the appropriate time interval for rainfall to accumulate, the moving cumulative rainfall data corresponding to time intervals ranging from 1 to 30 hours for all the typhoon events are first constructed. The cross-correlations between water level data and the moving cumulative rainfall data are then calculated. The results are as shown in Figure 4. It appears that, as expected, with the increase of time interval, the average CC between water level and the moving cumulative rainfall also increases. Correspondingly, the deviation between the maximum and the minimum CCs also generally decreases along with the increase of accumulation time interval. As shown in the figure, CC reaches the peak of around 0.9 corresponding to an accumulation interval at about 17 hours. This indicates that the water level at the study site is highly correlated to the moving cumulative rainfall with an accumulation interval of 17 hours, and the 17-h cumulative rainfall data are appropriate for use as the input to the ANFIS model.

To further examine the time lag between water level and 17-h cumulative rainfall, a cross-correlation analysis was conducted to calculate the CCs between water level and antecedent cumulative rainfall at time lags from 0 to 10 (10 minutes interval for each lag). As shown in Figure 5, there is an upward trend of average CC from lag (t) to lag (t-2), and the average CC begins to decline after lag (t-2). The peak CC level occurs at lag (t-2), where the average CC reaches 0.91, indicating water level is most correlated with the antecedent 17-h cumulative rainfall at 2 time-lags. In addition to lag (t-2), the CCs reach above 0.9 at lag (t), lag (t-1), and lag (t-3), suggesting that the cumulative rainfall

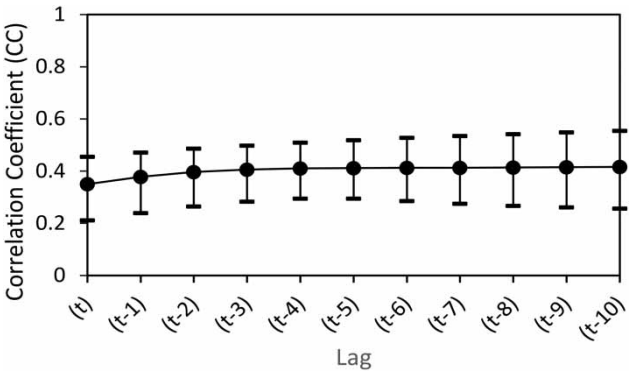

Figure 3 | Correlations between water-level and 10-min rainfall with various lags.

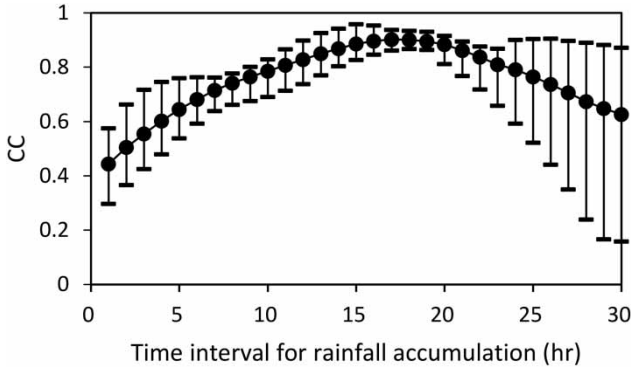

Figure 4 | Correlations between water-level and moving cumulative rainfall at various time intervals for rainfall accumulation.

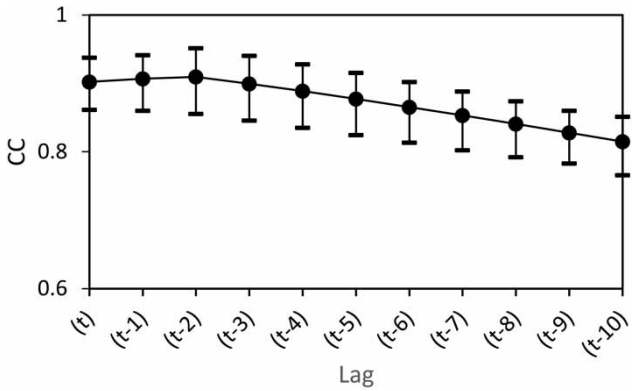

Figure 5 | Correlations between water-level and 17-h cumulative rainfall with various lags.

data at these time lags are all suited for use as the input data of the model.

Model construction

The simulation results of ANFIS depend on the model structure. Given a different combination of input variables, the simulation results may be diverse. In the present study, a total of 11 models are constructed associated with various input combinations. In the choice of input variables, two methods are adopted from previous research in the field. The first method is Sequential Time Series (Furundzic 1998; Tokar & Markus 2000; Riad *et al.* 2004; Chua *et al.* 2008), which is to input the cumulative rainfall data sequentially from the current time point to an earlier time point, that is, CR(t), CR(t-1), …, CR(t-m), where CR indicates the cumulative rainfall and m is determined by the maximum CC between water level and cumulative rainfall. The analysis results in the previous section show that water level is most correlated with the antecedent cumulative rainfall at lag(t-2). Hence, in Model 1, CR(t), CR(t-1), and CR(t-2) are adopted as inputs. Besides, the correlation between CR(t-3) and water level also reaches above 0.9, therefore CR(t), CR(t-1), CR(t-2), and CR(t-3) are utilized as inputs to Model 2. The second common method is Pruned Sequential Time Series (Mitra & Hayashi 2000; Nayak *et al.* 2007), which is to remove unnecessary variables and retain most correlated ones to avoid noise from redundant inputs. Following this method, CR(t-1) and CR(t-2) are selected as inputs in Model 3, CR(t-2) and CR(t-3) as inputs in Model 4, and CR(t-1), CR(t-2), and CR(t-3) as inputs in Model 5.

In order to analyze the influence of current water levels on inundation level forecasting, the settings of Models 1–5 are replicated by additionally considering the current water level data H(t) as an input to create another five models, Models 6–10. Moreover, we construct Model 11 that considers only H(t) as the input to provide the baseline data. Because QPESUMS forecasts rainfall for the next 72 hours, the cumulative rainfall forecast is available as the input data to predict future variations in water level. Take the water level forecast for the next 3 hours H(t + 18) (the time interval of each observation is 10 minutes) as an example. Model 1 will use CR(t + 18), CR(t + 17), and CR(t + 16) from QPESUMS to predict H(t + 18). In other models, the input data of cumulative rainfall are given in the same approach. On the other hand, there is no forecast data of water level and only the current water level transmitted from the gauging station is available. Therefore, in Models 6–11, the current water level is used as the input of water level. To predict H (t + 18), for example, the input variables of Model 6 are CR (t + 18), CR(t + 17), CR(t + 16), and H(t). The detailed input variables of all the 11 models are listed in Table 2. Based on their inputs, models M1–M5 refer to ANFIS-R models which use only rainfall data as inputs, and M6–M11 refer to ANFIS-B models which include water level data as inputs.

Following the approach of Rajurkar *et al.* (2002), the water level and cumulative rainfall data are standardized using the following equation:

$$y_n = 0.1 + 0.8\left(\frac{y_i - y_{min}}{y_{max} - y_{min}}\right) \tag{4}$$

where y_n is the standardized data; y_i denotes the original data; y_{max} and y_{min} are the maximum and minimum of the original data, respectively. After standardization, all the data ranges between 0.1 and 0.9. In the setting of ANFIS, Talei *et al.* (2010) found no significant improvement in forecast results when the number of membership functions is greater than 2. To reduce computation effort, the number of membership functions is set as 2 in this study. Nayak *et al.* (2004) pointed out that the type of membership function does not have a deterministic effect on model performance. A preliminary test shows that the triangular membership function performs well and is therefore adopted in the models.

Table 2 | Input variables of the ANFIS models

Model type	Model	Input variables				
	M1	CR(t + k)	CR(t + k-1)	CR(t + k-2)		
	M2	CR(t + k)	CR(t + k-1)	CR(t + k-2)	CR(t + k-3)	
ANFIS-R	M3		CR(t + k-1)	CR(t + k-2)		
	M4			CR(t + k-2)	CR(t + k-3)	
	M5		CR(t + k-1)	CR(t + k-2)	CR(t + k-3)	
	M6	CR(t + k)	CR(t + k-1)	CR(t + k-2)		H(t)
	M7	CR(t + k)	CR(t + k-1)	CR(t + k-2)	CR(t + k-3)	H(t)
ANFIS-B	M8		CR(t + k-1)	CR(t + k-2)		H(t)
	M9			CR(t + k-2)	CR(t + k-3)	H(t)
	M10		CR(t + k-1)	CR(t + k-2)	CR(t + k-3)	H(t)
	M11					H(t)

k: prediction horizon.

Evaluation indices

To compare the predicting capability between models, the following indices are employed to evaluate model performance.

Coefficient of efficiency

Coefficient of efficiency (CE) was proposed by Nash & Sutcliffe (1970) for the evaluation of a hydrologic model. CE is defined as follows:

$$\mathrm{CE} = 1 - \frac{\sum_{t=1}^{n_t} [y_{obs}(t) - y_{est}(t)]^2}{\sum_{t=1}^{n_t} [y_{obs}(t) - \bar{y}_{obs}]^2} \tag{5}$$

where y_{obs} and y_{est} respectively denote the observed and estimated water levels, $\bar{y}_{obs}$ is the average observed water level, and n_t is the number of data points. A CE value closer to 1 indicates a smaller difference between the estimated water level and the observed level.

Peak level error

$$\mathrm{PE} = \frac{|y_{p,obs} - y_{p,est}|}{y_{p,obs}} \tag{6}$$

where $y_{p,obs}$ and $y_{p,est}$ respectively denote the observed peak water level and the estimated peak water level. A peak level error (PE) value closer to 0 indicates a smaller difference between the estimated peak water level and the observed peak water level.

Relative time shift

It is shown in Talei & Chua (2012) that using time series data to forecast future variation is prone to suffer time shift error, such that the output hydrograph shifts from the observation by a certain amount of time. To examine the degree of the models in time shift error, the procedure of Talei *et al.* (2010) is adopted here. The predicted hydrograph by the model is shifted back in time by 1–18 time-steps and CE of the shifted hydrograph is calculated each time. The shift step at which the maximum CE is reached represents the time shift of the output hydrograph and is recorded as δ. The relative time shift (RTS) of the models is defined as follows:

$$\mathrm{RTS} = \frac{\bar{\delta}}{k} \tag{7}$$

where $\bar{\delta}$ denotes the event-averaged mean value of δ for all typhoons, and k is the prediction horizon (time step of prediction lead). RTS ranges between 0 and 1, where 0 indicates absence of the time shift phenomenon and 1 denotes complete shifting of the output hydrograph from the observation.

The ANFIS toolbox in MATLAB is utilized for model construction. After a preliminary study, Typhoon Usagi

was selected for calibration of the models. For each model, the indices introduced above are calculated for all typhoon events, and the results, including the event-averaged mean, the maximum, and the minimum in all events, are used as the basis for evaluating model performance.

RESULTS AND DISCUSSION

Characteristics of the models

The 11 models constructed above are employed to forecast inundation levels with prediction leads of 0.5 and 3 hours, i.e. $H(t+3)$ and $H(t+18)$, each respectively represents short and long prediction lead times. The evaluation results of the forecasts by the three indices are as shown in Figure 6. Among the three indices, CE is the higher the better, whereas both PE and RTS are the lower the better. Hence, PE and RTS are presented in the forms of 1-PE and 1-RTS in the figures to facilitate comparison. Figure 6(a)–6(c) show the performances of the 11 models in forecasting $H(t+3)$, and Figure 6(d)–6(f) show the results in forecasting $H(t+18)$. In these figures, circle dots indicate the event-averaged means, and the error bars represent the range of the indices for all events. The vertical dash line divides the 11 models into two groups. Models M1–M5 refers to

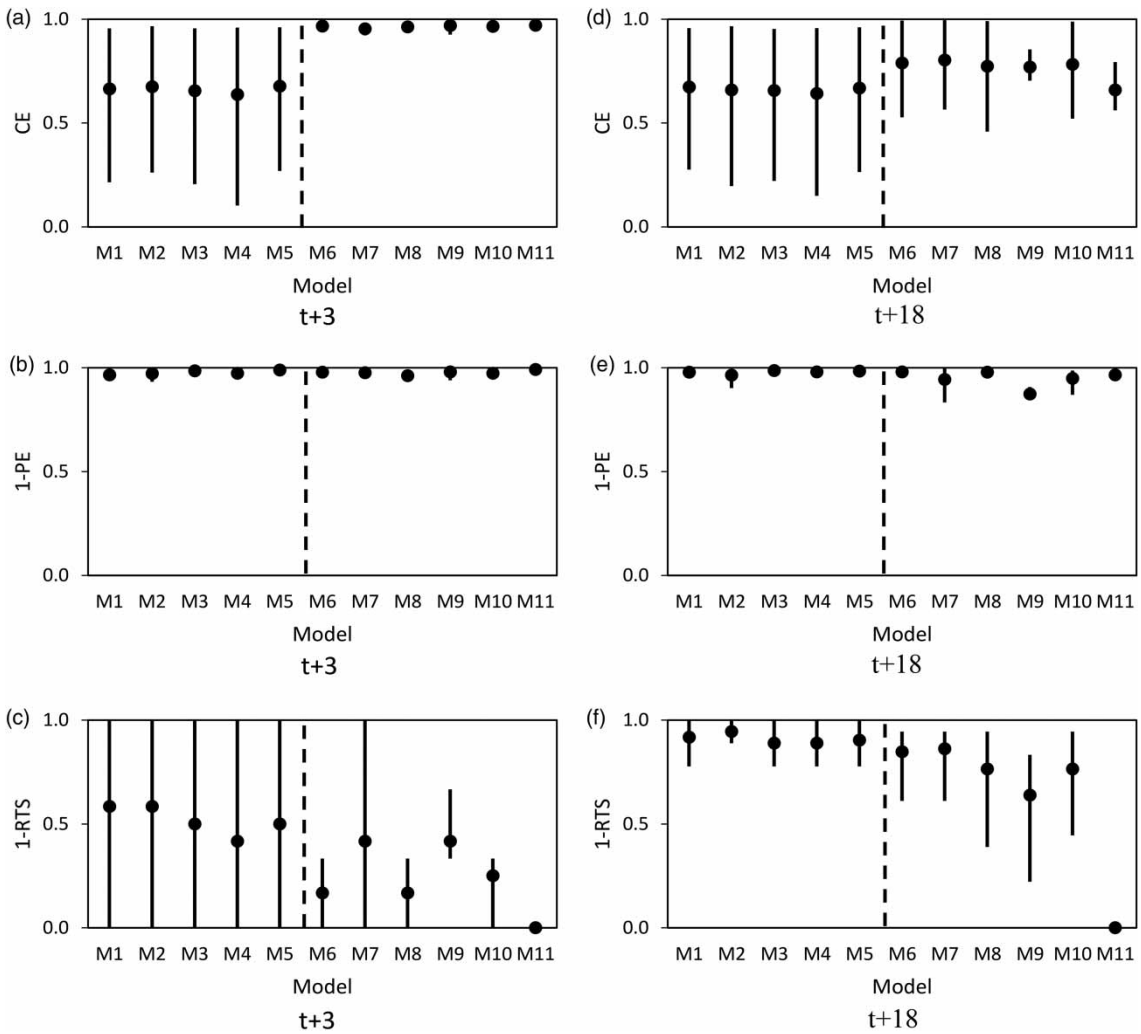

Figure 6 | Model performances on CE, PE, and RTS with prediction leads of $t+3$ and $t+18$.

ANFIS-R models that use only rainfall data as inputs, while models M6–M11 refers to ANFIS-B models that include H(t) in the inputs.

In terms of CE performance shown in Figure 6(a), ANFIS-B models (M6–M11) obviously outperform ANFIS-R models (M1–M5) in forecasting H(t + 3). The average CEs are all above 0.9, and the distributions are also concentrated. In contrast, the average CEs of ANFIS-R models (M1–M5) are about 0.7 with much wider distributions. Increasing the lead time to 3 hours (i.e. H(t + 18)), as shown in Figure 6(d), the average CEs of ANFIS-B models decline to about 0.8, and the distributions are also wider. However, their overall performances are still better compared to ANFIS-R models. This finding implies that the current water level H(t) has a considerable influence on inundation level prediction. Including H(t) as an input variable significantly improves the performance of ANFIS models in forecasting the inundation level for typhoons. The comparison of ANFIS-B models in Figure 6(d) shows that M6–M10 have similar levels of average CEs, and the CE of M11 is slightly lower than other ANFIS-B models. The reason for this is because M11 uses only the current water level H(t) as the input variable and forecasting with only H(t) will be less accurate than forecasting with both cumulative rainfall and water level data when giving a longer prediction lead time. The similar levels of average CE for M6–M10 might be due to the inputs of these models comprising of CR(t) through CR(t-3) which have rather comparable correlations to the water level, as shown in Figure 5. It should be noted that the distributions of CEs of ANFIS-R models in Figure 6(a) and 6(d) indicate that the forecasting performances for H(t + 3) are not obviously different from those for H(t + 18). The average CEs maintain at about 0.7, and the distributions do not vary greatly. It is because all ANFIS-R models use forecast rainfall data from QPESUMS as the input data, and hence is not much influenced by prediction lead time.

Figure 6(b) and 6(e) present the 1-PE performances of all the models when forecasting H(t + 3) and H(t + 18). As shown in Figure 6(b), the differences among all of the models in forecasting the peak water level at H(t + 3) are minimal. All the average 1-PE values reach above 0.95, and the distributions are quite concentrated. This demonstrates the good performance of the models at a short prediction lead time. If the lead time is extended to 3 hours, as shown in Figure 6(e), ANFIS-R models are not much affected, while ANFIS-B models' performances decline slightly but their 1-PE scores stay around 0.9. This indicates that all these models can deliver a good prediction accuracy for peak water level when given a long prediction lead.

Figure 6(c) and 6(f) compare the RTS of the 11 models when forecasting H(t + 3) and H(t + 18). As shown in Figure 6(c), when given a short prediction lead, ANFIS-R models have a slightly higher mean 1-RTS than ANFIS-B models. In other words, the time shift phenomenon is less evident in the forecasts of ANFIS-R models. On the other hand, ANFIS-B models, which consist of H(t) as an input, suffer a more serious time shift error, as indicated by the lower 1-RTS in Figure 6(c). The time shift error is most serious in M11 which has H(t) as its only input variable. Lacking the rainfall data in the inputs, the 1-RTS of M11 is 0 for all the events, suggesting that its output hydrograph is shifting in time from the observation with exactly the prediction lead. This is also observed in Figure 6(f) when M11 forecasts H(t + 18) at a longer lead time. In the comparison of 1-RTS between ANFIS-R and ANFIS-B models at a longer lead time, as shown in Figure 6(f), it appears that ANFIS-R models still outperform ANFIS-B models with generally higher average 1-RTS scores.

In summary, ANFIS-B models generally outperform ANFIS-R models in terms of CE but are inferior to them in terms of RTS, an indicator of the time shift problem. As to PE, ANFIS-R models are slightly better than ANFIS-B models but the differences are not significant.

Model comparison

To conduct a comprehensive evaluation of these models, each model is rated by the following index (Talei *et al.* 2010):

$$R_j = a_{1,j}\overline{CE}_j + a_{2,j}(1 - \overline{PE}_j) + a_{3,j}(1 - \overline{RTS}_j), \quad j = 1, \cdots, 11 \tag{8}$$

where the subscript j indicates model id; $a_{1,j}$, $a_{2,j}$, and $a_{3,j}$ respectively take into account the diversity of CE, PE, and

RTS for model rating, and are defined as follows:

$$a_{i,j} = 1.5 - \frac{d_{i,j}}{d_{i,max}},\ i = 1,\ 2,\ 3 \text{ and } j = 1, \cdots,\ 11 \qquad (9)$$

where $d_{i,j}$ denotes the difference between the maximum and minimum values of index i for model j, and it is normalized using $d_{i,max}$, the maximum among all the 11 $d_{i,j}$ values. $d_{i,j}$ reflects the diversity of the typhoon events on index i for model j. If $d_{i,j}$ is large, $a_{i,j}$ declines according to Equation (9), causing a penalty effect on R_j and the overall score of the model deteriorates.

Table 3 shows the evaluation result for the 11 models in forecasting H(t + 18). As shown in the table, model M6 achieves the highest score in R, followed by model M4 with the second highest score. The performance of these two models is examined, as presented in Figure 7(a)–7(c) showing the variations in CE, 1-PE, and 1-RTS under various prediction leads, respectively. For comparison, the result of M11 which uses only H(t) as input is also presented in the figures. As shown in Figure 7(a), both M6 and M11 deliver an average CE above 0.9 at t + 3, but their CEs decline with the increase of prediction lead. Compared to M11, the decline of M6's CE is relatively slower. At a prediction lead of t + 18, M6 delivers an average CE near 0.8, whereas M11's average CE has dropped to about 0.6. M4 is generally not affected by prediction lead, as its average CE stays between 0.6 and 0.7.

Figure 7(b) shows the comparison of 1-PE over various prediction leads. M4, M6, and M11 all have a 1-PE value above 0.95 across different leads, and the differences between models are minimal. Overall, M6 is inferior to M4 in terms of PE. It is noted that M11 has a higher 1-PE compared to M4 and M6 at a shorter prediction horizon (t + 3–t + 12). However, in terms of 1-RTS as shown in Figure 7(c), M11 is all zero across different prediction leads, suggesting that M11's forecast results are very likely the time-shifted input hydrograph. Figure 7(c) also shows that the 1-RTS scores of M4 and M6 increase with the increase of prediction leads. Overall, M4 is superior to M6, but the difference becomes minimal at t + 18, where both have a 1-RTS above 0.8, indicating no serious time shift in their predictions.

Models M4 and M6 are compared with other approaches based on Auto-Regressive models with Exogenous input (ARX, Box & Jenkins 1976) and Nonlinear ARX with Wavelet function (NLARX-W, Ouyang 2016b). Both ARX and NLARX-W models use the same input variables as M6 (i.e. H(t) and CR(t + k) through CR((t + k-2)) and are calibrated using the same typhoon data. The mean CE, PE, and RTS averaged over the validated events are calculated and the results are as shown in Figure 8(a)–8(c). In the comparison of CE, as shown in Figure 8(a), M6 shows superior performance over ARX and NLARX-W models. On the other hand, M4 is a little less than the ARX-based models, but the difference is not very significant. It should be noted that M4 employs only rainfall data as inputs, while ARX and NLARX-W use both rainfall and water level data

Table 3 | Comparison of model performance

Model	M1	M2	M3	M4	M5	M6	M7	M8	M9	M10	M11
$\overline{CE}$	0.67	0.66	0.66	0.64	0.67	0.79	0.80	0.77	0.77	0.78	0.66
$1 - \overline{PE}$	0.98	0.97	0.99	0.98	0.98	0.98	0.94	0.98	0.87	0.95	0.97
$1 - \overline{RTS}$	0.92	0.94	0.89	0.89	0.90	0.85	0.86	0.76	0.64	0.76	0.00
a_{CE}	0.66	0.55	0.59	0.50	0.64	0.92	0.97	0.84	1.31	0.92	1.21
a_{PE}	1.28	0.95	1.39	1.50	1.30	1.39	0.50	1.39	1.16	0.80	1.50
a_{RTS}	1.14	1.32	1.14	1.14	1.14	0.95	0.95	0.59	0.50	0.68	1.50
R_{CE}	0.44	0.36	0.39	0.32	0.43	0.73	0.78	0.65	1.01	0.72	0.80
R_{PE}	1.25	0.92	1.38	1.47	1.28	1.36	0.47	1.37	1.02	0.76	1.45
R_{RTS}	1.04	1.24	1.01	11	1.03	0.81	0.82	0.45	0.32	0.52	0.00
R	2.74	2.53	2.78	2.80[a]	2.73	2.90[b]	2.07	2.47	2.35	2.00	2.25

[a]Second highest score.
[b]Highest score.

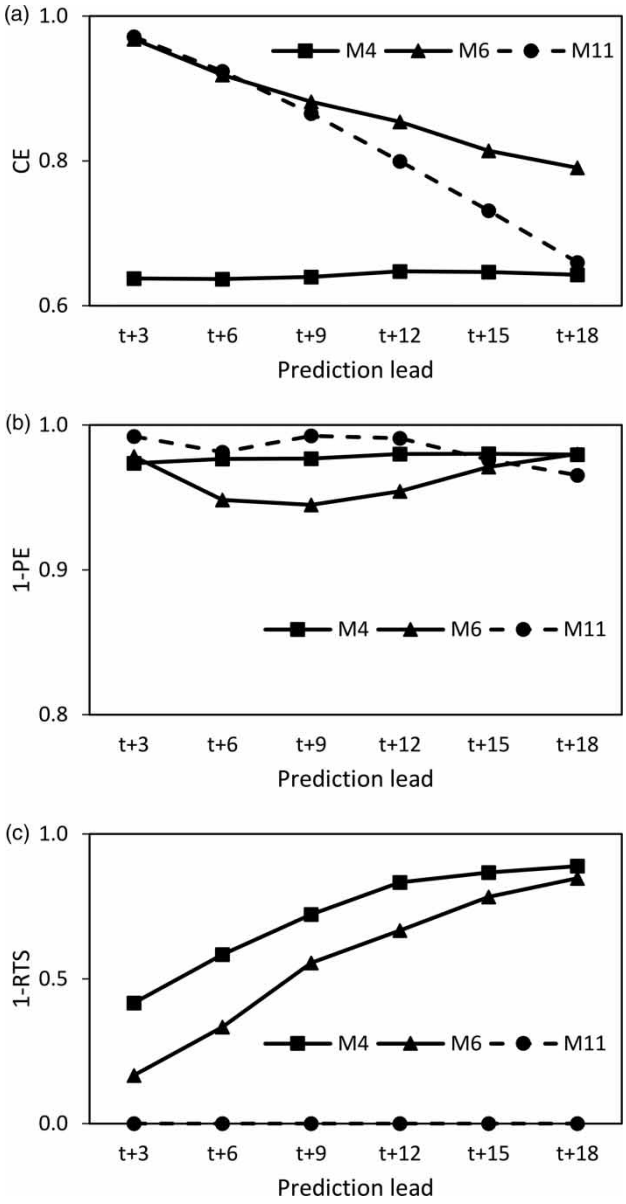

Figure 7 | Performances of M4, M6, and M11 at various prediction leads (a) CE, (b) 1-PE, (c) 1-RTS.

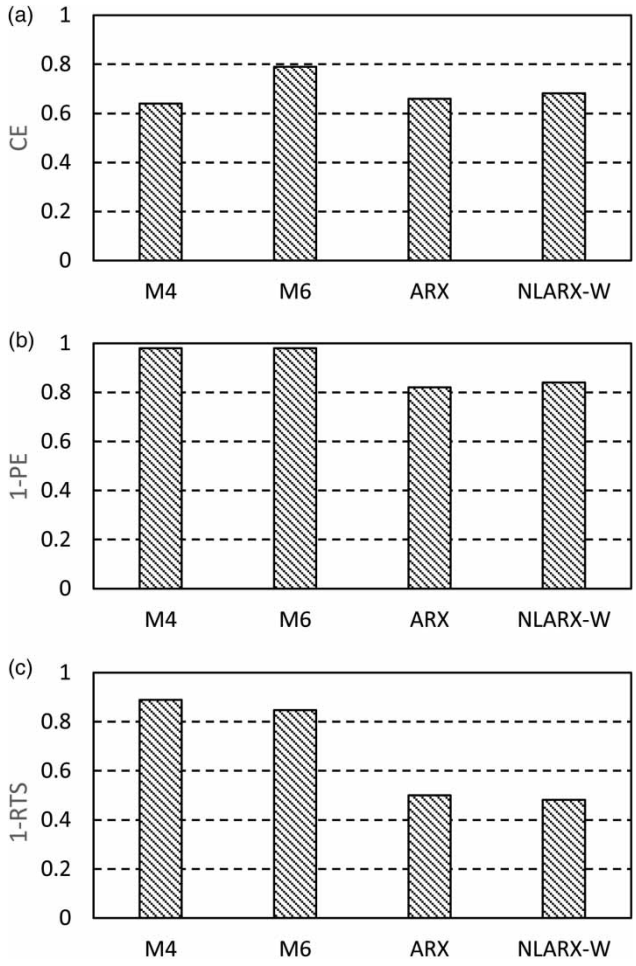

Figure 8 | Comparison of M4 and M6 to ARX-based models (a) CE, (b) 1-PE, (c) 1-RTS (prediction lead: t + 18).

in the inputs. Still, as can be seen in Figure 8(a), M4 is able to reach comparable CE performance with ARX-based models by using lesser inputs. Figure 8(b) shows the comparison of M4 and M6 to ARX and NLARX-W models on the performance of 1-PE. As seen, both M4 and M6 outperform the ARX-based models with higher 1-PE scores, indicating better performance in terms of peak water level prediction. Similar results are presented in Figure 8(c) for 1-RTS performance. As seen in the figure, both M4 and M6 achieve much higher 1-RTS scores than the ARX-based models, signifying less time shift in their predictions.

In summary, M6 as the best ANFIS-B model shows superior performance to ARX-based models on all the three indices. M4 as the best ANFIS-R model presents a comparable performance to ARX-based models in terms of CE and much better performance on PE and RTS. It is noted that, as M4 employs only rainfall data as inputs, this promising result renders the ANFIS-R model favorable for use in areas lacking water level observations.

Attempts on improving RTS

The above explorations show that, in general, M6 as the best ANFIS-B model delivers good performances except in RTS

Table 4 | M6-extended models

Model	Input variables						
M12	CR(t + k)	CR(t + k-1)	CR(t + k-2)	H(t)	H(t-1)		
M13	CR(t + k)	CR(t + k-1)	CR(t + k-2)	H(t)	H(t-1)	H(t-2)	
M14	CR(t + k)	CR(t + k-1)	CR(t + k-2)	H(t)	H(t-1)	H(t-2)	H(t-3)

at short prediction lead. It is speculated that including more antecedent water level data in the inputs might provide information on the rate of change in water levels, which in turn might improve the RTS performance of model M6. Thus, three extended models are created based on M6's model structure, namely M12, M13, and M14. In these new models, the antecedent water levels H(t-1)–H(t-3) are also considered as input variables to examine the effect of these variables on water level forecasts. M12 has similar inputs with M6 but takes account of one more input H(t-1). Similarly, M13 has two more inputs, H(t-1) and H(t-2); and M14 has three more inputs, H(t-1), H(t-2), and H(t-3). The input variables of these three extended models are as listed in Table 4. The performances of M6, M12, M13, and M14 on CE, 1-PE, and 1-RTS are respectively compared in Figure 9(a)–9(c). Results indicate that after including antecedent water levels as input variables, surprisingly, these extended models not only show no improvement on RTS but also exhibit, in general, poorer performance in terms of CE and PE, as shown in Figure 9(a)–9(c). That is to say, including antecedent water levels as input variables cannot enhance the forecast capability of models but will rather drag down their performances. This might be due to redundant information somehow being provided to the ANFIS models. Similar results have also been reported by Mitra & Hayashi (2000).

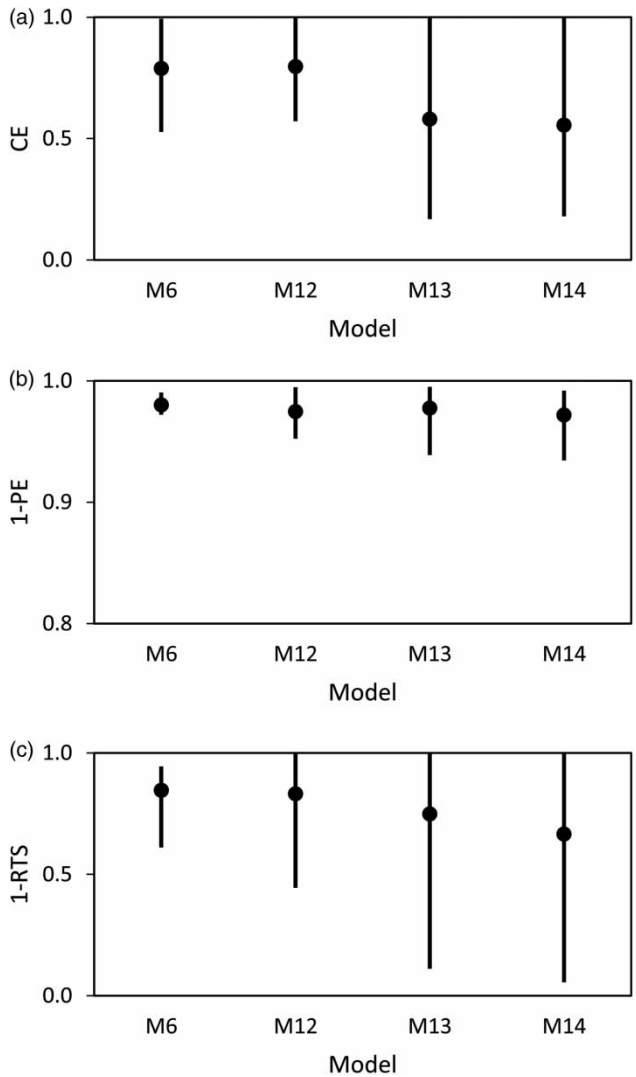

Figure 9 | Comparison between M6 and its extended models (a) CE, (b) 1-PE, (c) 1-RTS (prediction lead: t + 18).

Figure 10 shows the comparison between the estimated water level predicted by M6 and the observation data of Typhoon Soudelor at different prediction leads from t + 3–t + 18. As shown in Figure 10(a), at a prediction lead of t + 3 (0.5 h), the estimated water level is very close to the observation, showing very good predictions. Increasing the prediction lead to t + 6 (1 h), as shown in Figure 10(b), the time shift error is seemingly present in the rising limb of the predicted hydrograph, but the estimated water level in the recession limb is quite accurate. With prediction lead increased to t + 9 (1.5 h), as shown in Figure 10(c), the time shift error worsens in the estimated rise of water level, also the estimated fall of water level is earlier than the observation. In further comparison with a continuously

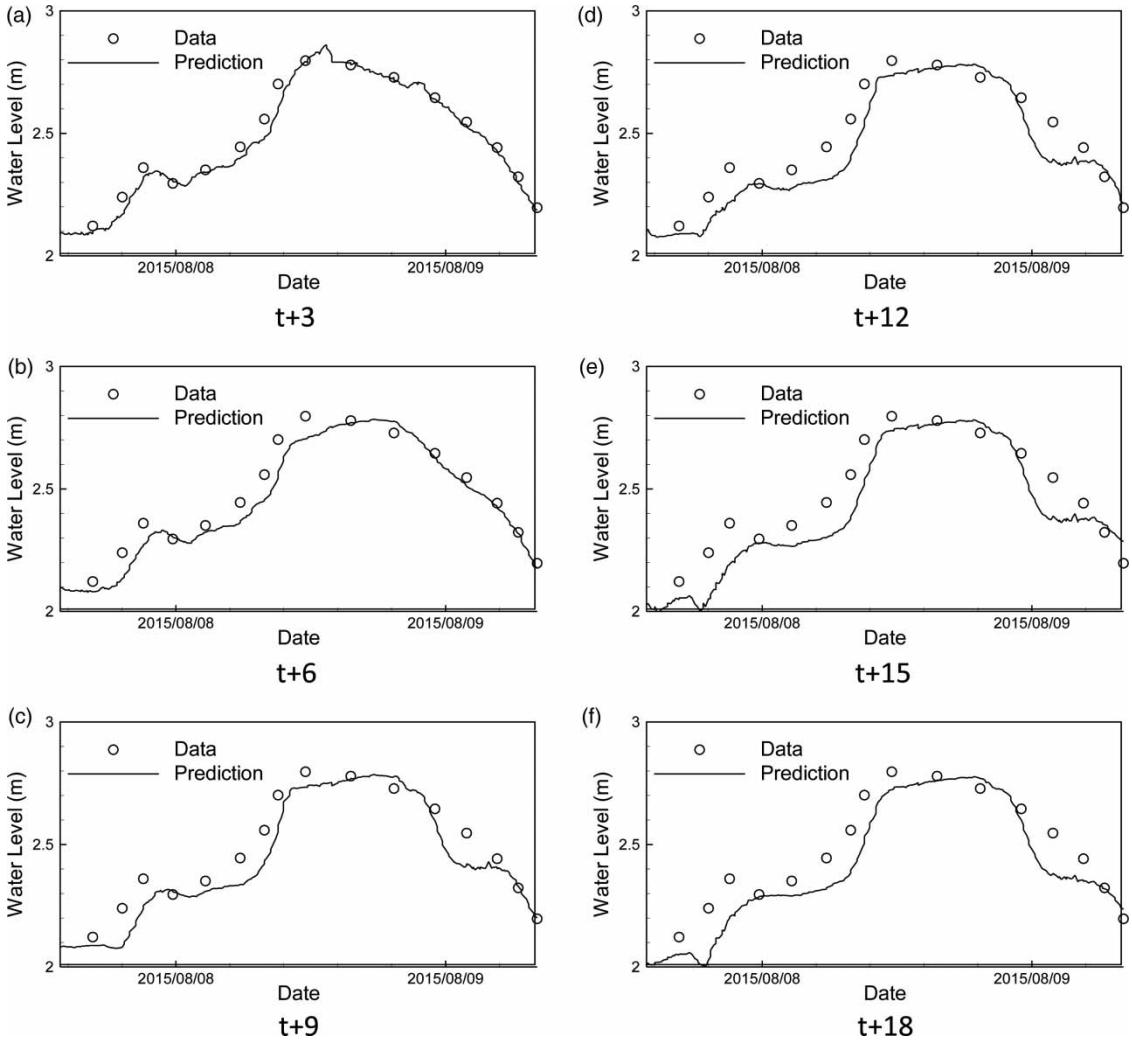

Figure 10 | Comparison between M6 estimated water level and observed water level at various prediction leads (Typhoon Soudelor).

extended prediction leads (t + 12–t + 18), the model produces forecast results that are generally similar without a greater time shift in the rising limb of the hydrograph and a greater earlier fall in the recession limb. Overall, the model delivers a satisfactory performance in inundation level forecast.

Sensitivity analysis

The rainfall forecast from QPESUMS is used as model inputs in the present study. The accuracy of rainfall forecast is an important factor which affects the result of the water level prediction. A sensitivity analysis was thus carried out to investigate the effect of rainfall uncertainty on model predictions. Error statistics by means of CC (R), root mean square error (RMSE), bias (B), and scatter index (SI) are assessed, which are computed as:

$$R = \frac{\sum_{t=1}^{n} (y_{obs}(t) - \bar{y}_{obs})(y_{est}(t) - \bar{y}_{est})}{\sqrt{\sum_{t=1}^{n} (y_{obs}(t) - \bar{y}_{obs})^2 \sum_{t=1}^{n} (y_{est}(t) - \bar{y}_{est})^2}} \tag{10}$$

$$RMSE = \sqrt{\frac{\sum_{t=1}^{n} [y_{obs}(t) - y_{est}(t)]^2}{n}}. \tag{11}$$

$$B = \frac{\sum_{t=1}^{n} [y_{obs}(t) - y_{est}(t)]}{n} \tag{12}$$

$$SI = \frac{RMSE}{\bar{y}_{obs}} \tag{13}$$

The sensitivity of each model on the rainfall data is examined by perturbing the rainfall data by 5% while the water level data remains fixed. The absolute differences in the four error indices, R, RMSE, B, and SI associated with the perturbed rainfall data are calculated. The results are shown in Table 5, as designated by the perturbed parameter of CR. It is noted that M11 does not use rainfall data as an input and thus is excluded in the sensitivity analysis associated with CR. As shown in the table, in general, ANFIS-R models appear to be more sensitive to the variation of rainfall data than ANFIS-B models, as designated by the generally greater absolute differences in the error indices (i.e. $|\delta_R|$, $|\delta_{RMSE}|$, $|\delta_B|$, and $|\delta_{SI}|$) for ANFIS-R models. As shown in Table 5, for 5% of rainfall variations, $|\delta_{RMSE}|$ are around 0.10–0.12 m for ANFIS-R models, whereas they are only 0.01–0.015 m for ANFIS-B models.

Table 5 | Sensitivities of the models to the input variables by 5% of perturbations

Model type	Model	Perturbed parameter	$\lvert\delta_R\rvert$	$\lvert\delta_{RMSE}\rvert$ (m)	$\lvert\delta_B\rvert$ (m)	$\lvert\delta_{SI}\rvert$
ANFIS-R	M1	CR	0.005	0.113	0.12	0.052
	M2	CR	0.017	0.111	0.112	0.051
	M3	CR	0.009	0.104	0.109	0.048
	M4	CR	0.008	0.100	0.113	0.046
	M5	CR	0.013	0.108	0.118	0.050
ANFIS-B	M6	CR	0.001	0.011	0.020	0.005
		H	0.004	0.104	0.086	0.048
	M7	CR	0.003	0.015	0.026	0.007
		H	0.014	0.053	0.068	0.047
	M8	CR	0.003	0.013	0.022	0.006
		H	0.008	0.039	0.083	0.048
	M9	CR	0.002	0.014	0.03	0.006
		H	0.006	0.050	0.082	0.051
	M10	CR	0.002	0.012	0.024	0.005
		H	0.012	0.053	0.080	0.045
	M11	H	0.122	0.052	0.165	0.054
	M12	CR	0.002	0.011	0.024	0.005
		H	0.004	0.048	0.088	0.047
	M13	CR	0.001	0.012	0.022	0.005
		H	0.006	0.047	0.088	0.050
	M14	CR	0.001	0.011	0.024	0.005
		H	0.006	0.053	0.111	0.050

The effect of water level input on the forecast is also investigated via the sensitivity analysis. Water level forecasts associated with 5% of perturbation on the water level input are conducted, and the absolute differences in the four error indices, R, RMSE, B, and SI are calculated. The results are shown in Table 5, as designated by the perturbed parameter of H. It is noted that in the table only ANFIS-B models are subjected to the sensitivity analysis associated with H because ANFIS-R models use rainfall data as inputs only. As shown in Table 5, it appears that ANFIS-B models (M6–M14) are, in general, more sensitive to the water level data (H) than to the rainfall (CR), as signified by the greater absolute differences in the four error indices of $|\delta_R|$, $|\delta_{RMSE}|$, $|\delta_B|$, and $|\delta_{SI}|$ resulting from perturbations on H than on CR. As shown, for 5% of perturbations on H, $|\delta_{RMSE}|$ of the model predictions are in the range of 0.04–0.10 m, whereas they are only around 0.01–0.015 m with the same level of variations in rainfall data. This explains the much greater time shift error in the forecast of ANFIS-B models and also the above-mentioned failure in the attempt to improve RTS by including more antecedent water level data in the inputs. Since ANFIS-B makes use of both water level in current time and rainfall predictions as inputs to forecast future water level, being highly sensitive to water level data, the model relies more on the information from current water level than from rainfall prediction. As a result, the predicted water level tends to be lagged behind the water level observation as it happens, hence producing the time shift error. Including more antecedent water level data in the inputs will only cause the model to rely more on past water level than on rainfall prediction, and consequently deteriorates the time shift error even more. ANFIS-R models, on the other hand, spare this deficiency because they employ only rainfall predictions in the inputs. It is noted that, since the models were trained using measured rainfall but run using projected rainfall, in practice there will be errors on account of the rainfall forecast as well. Thus, the quality of rainfall forecast will affect the accuracy of the model prediction as the model cannot account for errors that are inherent in the inputs. The accuracy of the rainfall forecast, which it is believed will improve

in time, is nevertheless beyond the scope of the present study.

CONCLUSIONS

The characteristics of ANFIS-based models for typhoon inundation level forecasts have been explored. Based on correlation analysis on rainfall and water level data in the study area, two types of ANFIS models were proposed: ANFIS-R which uses only rainfall data as inputs to cope with cases where water level surveillance programs have ceased to continue, and ANFIS-B which takes in both rainfall and water level data as inputs. In total, 11 models were constructed and the forecast accuracy, the PE, and the time shift error for each of the models were assessed in terms of CE, PE, and RTS. The results show that, while ANFIS-R models generally have lower CE performance than ANFIS-B models, they nevertheless outperform ANFIS-B models in terms of PE and RTS with lesser peak error and time shift.

The models were rated by considering all three indices as well as the diversity of these indices, and the best ones achieving the highest scores (M4 and M6 for ANFIS-R and ANFIS-B models, respectively) were selected and compared to the traditional ARX-based models. The results show that the best ANFIS-B model exhibits superior performance over the ARX-based models in terms of all the three indices of CE, PE, and RTS. The best ANFIS-R model displays comparable CE score and superior performance on PE and RTS compared to the ARX-based models. As the ANFIS-R uses only rainfall data as inputs while ARX-based models employ both rainfall and water level data, this result demonstrates the superiority of the proposed ANFIS-R model and renders it favorable for use in areas where water level monitoring is lacking.

In an attempt to improve the RTS performance of ANFIS-B model, extended models that include antecedent water levels as extra inputs were tested. The results, however, show that including antecedent water levels in the model inputs will not improve the RTS performance in the forecasts. Instead, it will result in reduced model performances on all the three indices of CE, PE, and RTS. Results of sensitivity analysis show that the forecasts of ANFIS-B are more sensitive to the uncertainty in water level input than in rainfall input, which consequently results in lags in the water level forecasts. This explains the greater time shift error in the forecasts of ANFIS-B than in ANFIS-R, as well as the worse RTS in the extended models when including more antecedent water level data in the inputs.

ACKNOWLEDGEMENTS

This research was supported by the Ministry of Science and Technology in Taiwan under grant No. MOST 105-2625-M-197-001. Support from the Water Resources Agency in Taiwan is also acknowledged.

REFERENCES

Babel, M. S., Sirisena, T. A. J. G. & Singhrattna, N. 2016 Incorporating large-scale atmospheric variables in long-term seasonal rainfall forecasting using artificial neural networks: an application to the Ping Basin in Thailand. *Hydrol. Res.* DOI: 10.2166/nh.2016.212.

Box, G. E. & Jenkins, G. M. 1976 *Time Series Analysis: Forecasting and Control,* revised edn. John Wiley & Sons, Hoboken, NJ.

Chang, L. C. & Chang, F. J. 2001 Intelligent control for modelling of real-time reservoir operation. *Hydrol. Process.* **15** (9), 1621–1634.

Chang, F. J. & Chang, Y. T. 2006 Adaptive neuro-fuzzy inference system for prediction of water level in reservoir. *Adv. Water Resour.* **29** (1), 1–10.

Chang, Y. T., Chang, L. C. & Chang, F. J. 2005 Intelligent control for modeling of real-time reservoir operation, part II: artificial neural network with operating rule curves. *Hydrol. Process.* **19** (7), 1431–1444.

Chua, L. H., Wong, T. S. & Sriramula, L. K. 2008 Comparison between kinematic wave and artificial neural network models in event-based runoff simulation for an overland plane. *J. Hydrol.* **357** (3), 337–348.

Fayaed, S. S., El-Shafie, A., Alsulami, H. M., Jaafar, O., Mukhlisin, M. & El-Shafie, A. 2015 Augmentation of an artificial neural network and modified stochastic dynamic programing model for optimal release policy. *Hydrol. Res.* **46** (5), 689–704.

Feng, Y., Gong, D., Mei, X. & Cui, N. 2016 Estimation of maize evapotranspiration using extreme learning machine and generalized regression neural network on the China Loess Plateau. *Hydrol. Res.* DOI:10.2166/nh.2016.099.

Furundzic, D. 1998 Application example of neural networks for time series analysis: rainfall–runoff modeling. *Signal Process.* **64** (3), 383–396.

Gayen, A. K. 1951 The frequency distribution of the product-moment correlation coefficient in random samples of any

size drawn from non-normal universes. *Biometrika* **38** (1/2), 219–247.

Gorgij, A. D., Kisi, O. & Moghaddam, A. A. 2016 Groundwater budget forecasting, using hybrid wavelet-ANN-GP modelling: a case study of Azarshahr Plain, East Azerbaijan, Iran. *Hydrol. Res.* **48** (2), 455–467.

Gourley, J. J., Maddox, R. A., Howard, K. W. & Burgess, D. W. 2002 An exploratory multisensor technique for quantitative estimation of stratiform rainfall. *J. Hydrometeorol.* **3** (2), 166–180.

Granata, F., Gargano, R. & de Marinis, G. 2016 Support vector regression for rainfall-runoff modeling in urban drainage: a comparison with the EPA's storm water management model. *Water* **8** (3), 69.

Jang, J. S. R. 1993 ANFIS: adaptive-network-based fuzzy inference system. *IEEE Trans. Syst. Man Cybern.* **23** (3), 665–685.

Li, Y. L., Zhang, Q., Werner, A. D. & Yao, J. 2015 Investigating a complex lake-catchment-river system using artificial neural networks: Poyang Lake (China). *Hydrol. Res.* **46** (6), 912–928.

Li, X., Sha, J. & Wang, Z. L. 2016 A comparative study of multiple linear regression, artificial neural network and support vector machine for the prediction of dissolved oxygen. *Hydrol. Res.* DOI:10.2166/nh.2016.149.

Mamdani, E. H. 1974 Application of fuzzy algorithms for control of simple dynamic plant. *Proc. Inst. Elec. Eng.* **121** (12), 1585–1588.

Marinos, P. N. 1969 Fuzzy logic and its application to switching systems. *IEEE Trans. Comput.* **4**, 343–348.

Mitra, S. & Hayashi, Y. 2000 Neuro-fuzzy rule generation: survey in soft computing framework. *IEEE Trans. Neural Netw.* **11** (3), 748–768.

Moeini, R., Afshar, A. & Afshar, M. 2011 Fuzzy rule-based model for hydropower reservoirs operation. *Int. J. Electr. Power Energy Syst.* **33** (2), 171–178.

Mousavi, S. J., Ponnambalam, K. & Karray, F. 2007 Inferring operating rules for reservoir operations using fuzzy regression and ANFIS. *Fuzzy Sets Syst.* **158** (10), 1064–1082.

Najafzadeh, M. & Bonakdari, H. 2016 Application of a neuro-fuzzy GMDH model for predicting the velocity at limit of deposition in storm sewers. *J. Pipeline Syst. Eng. Pract.* http://dx.doi.org/10.1061/(ASCE)PS.1949-1204.0000249.

Najafzadeh, M. & Sattar, A. M. 2015 Neuro-fuzzy GMDH approach to predict longitudinal dispersion in water networks. *Water Resour. Manage.* **29** (7), 2205–2219.

Najafzadeh, M. & Tafarojnoruz, A. 2016 Evaluation of neuro-fuzzy GMDH-based particle swarm optimization to predict longitudinal dispersion coefficient in rivers. *Environ. Earth Sci.* **75** (2), 157.

Napolitano, G., See, L., Calvo, B., Savi, F. & Heppenstall, A. 2010 A conceptual and neural network model for real-time flood forecasting of the Tiber River in Rome. *Phys. Chem. Earth A/B/C* **35** (3), 187–194.

Nash, J. E. & Sutcliffe, J. V. 1970 River flow forecasting through conceptual models. Part I – A discussion of principles. *J. Hydrol.* **10** (3), 282–290.

Nayak, P. C., Sudheer, K. P., Rangan, D. M. & Ramasastri, K. S. 2004 A neuro-fuzzy computing technique for modeling hydrological time series. *J. Hydrol.* **291** (1), 52–66.

Nayak, P. C., Sudheer, K. P. & Jain, S. K. 2007 Rainfall-runoff modeling through hybrid intelligent system. *Water Resour. Res.* **43** (7), DOI: 10.1029/2006WR004930.

Ouyang, H. T. 2016a Multi-objective optimization of typhoon inundation forecast models with cross-site structures for a water-level gauging network by integrating ARMAX with a genetic algorithm. *Nat. Hazards Earth Syst. Sci.* **16** (8), 1897–1909.

Ouyang, H. T. 2016b Optimization of autoregressive, exogenous inputs-based typhoon inundation forecasting models using a multi-objective genetic algorithm. *Eng. Optim.* DOI:10.1080/0305215X.2016.1230207.

Pan, T. Y., Chang, L. Y., Lai, J. S., Chang, H. K., Lee, C. S. & Tan, Y. C. 2014 Coupling typhoon rainfall forecasting with overland-flow modeling for early warning of inundation. *Nat. Hazards* **70** (3), 1763–1793.

Rajurkar, M. P., Kothyari, U. C. & Chaube, U. C. 2002 Artificial neural networks for daily rainfall–runoff modelling. *Hydrol. Sci. J.* **47** (6), 865–877.

Riad, S., Mania, J., Bouchaou, L. & Najjar, Y. 2004 Predicting catchment flow in a semi-arid region via an artificial neural network technique. *Hydrol. Process.* **18** (13), 2387–2393.

Takagi, T. & Sugeno, M. 1985 Fuzzy identification of systems and its applications to modeling and control. *IEEE Trans. Syst. Man Cybernet.* **1**, 116–132.

Talei, A. & Chua, L. H. 2012 Influence of lag time on event-based rainfall–runoff modeling using the data driven approach. *J. Hydrol.* **438**, 223–233.

Talei, A., Chua, L. H. C. & Wong, T. S. 2010 Evaluation of rainfall and discharge inputs used by daptive network-based fuzzy inference systems (ANFIS) in rainfall–runoff modeling. *J. Hydrol.* **391** (3), 248–262.

Tokar, A. S. & Markus, M. 2000 Precipitation-runoff modeling using artificial neural networks and conceptual models. *J. Hydrol. Eng.* **5** (2), 156–161.

Yin, Z., Wen, X., Feng, Q., He, Z., Zou, S. & Yang, L. 2016 Integrating genetic algorithm and support vector machine for modeling daily reference evapotranspiration in a semi-arid mountain area. *Hydrol. Res.* DOI:10.2166/nh.2016.205.

Zadeh, L. A. 1971 Quantitative fuzzy semantics. *Inf. Sci.* **3** (2), 159–176.

Zounemat-Kermani, M. 2016 Assessment of several nonlinear methods in forecasting suspended sediment concentration in streams. *Hydrol. Res.* DOI: 10.2166/nh.2016.219.

First received 12 January 2017; accepted in revised form 23 March 2017. Available online 12 May 2017